Title	The influence of iso-butene kinetics on the reactivity of di-isobutylene and iso-octane
Author(s)	Lokachari, Nitin; Panigrahy, Snehasish; Kukkadapu, Goutham; Gihun, Kim; Vasu, Subith S.; Pitz, William J.; Curran, Henry J.
Publication Date	2020-09-06
Publication Information	Lokachari, Nitin, Panigrahy, Snehasish, Kukkadapu, Goutham, Kim, Gihun, Vasu, Subith S., Pitz, William J., & Curran, Henry J. (2020). The influence of iso-butene kinetics on the reactivity of di-isobutylene and iso-octane. Combustion and Flame, 222, 186-195. doi:https://doi.org/10.1016/j.combustflame.2020.08.007
Publisher	Elsevier
Link to publisher's version	https://doi.org/10.1016/j.combustflame.2020.08.007
Item record	http://hdl.handle.net/10379/16439
DOI	http://dx.doi.org/10.1016/j.combustflame.2020.08.007

The influence of isobutene kinetics on the reactivity of di-isobutylene and iso-octane

Nitin Lokachari[1,*], Snehasish Panigrahy[1], Goutham Kukkadapu[2], Gihun Kim[3], Subith Vasu[3], William J. Pitz[2], Henry J. Curran[1]

[1]Combustion Chemistry Centre, School of Chemistry, Ryan Institute, MaREI, National University of Ireland Galway, Ireland

[2]Lawrence Livermore National Laboratory, Livermore, CA 94551, USA

[3]Center for Advanced Turbomachinery and Energy Research (CATER), Mechanical and Aerospace Engineering, University of Central Florida, Orlando, FL 32816, USA

*Corresponding author: n.lokachari1@nuigalway.ie

Abstract

The continuous development of a core $C_0 – C_4$ kinetic mechanism generally involves updating it using reliable kinetics, thermodynamics and may also involve the inclusion of missing pathways to improve the integrity, prediction accuracy and applicability of the mechanism over a wider range of combustion relevant conditions. Accurate kinetic description of the core mechanism can be substantial in accurate predictions of higher hydrocarbon combustion models as the consumption of these species rely heavily on the core mechanism. This study was motivated by severe under prediction in the reactivity of the high temperature experimental targets of di-isobutylene (DIB), an important component used in surrogate fuel formulations. It is worth noting that isobutene (iC_4H_8) laminar burning velocities are also severely under-predicted in the recent publication of Zhou et al. [1], which is regarded as a critical fragment formed in the decomposition of DIB, that dictates its fate. We discuss the latest developments to the isobutene kinetics and illustrate the influence these updates have on the oxidation of higher order hydrocarbons, such as DIB and iso-octane (iC_8H_{18}). Improving the kinetic accuracy of the $C_0 – C_4$ core mechanism improved not only the iC_4H_8 predictions but also the predictions of higher hydrocarbons which hierarchically rely on it, for instance, the peak flame speeds for specific cases of iso-octane, iso-butene and di-isobutylene have improved by 3, 6, 12 cm s^{-1}, respectively. In addition, the new iC_4H_8 model is in excellent agreement with the new laminar burning velocity

measurements taken in this study at 1 atm and 428 K. Contribution of the new iC_4H_8 kinetics alone for the improvement in the LBV prediction is significant, in particular $\dot{C}_3H_5$-t + $\dot{C}H_3$ = $i\dot{C}_4H_7$ + $\dot{H}$ and iC_4H_8 = $i\dot{C}_4H_7$ + $\dot{H}$ reactions are very sensitive at high temperatures. In addition, the new isobutene model is in very good agreement with experimental ignition delay times and species profiles measured during pyrolysis and oxidation conditions.

Keywords: combustion kinetics, iso-butene, di-isobutylene, iso-octane, laminar burning velocity

1. Introduction

A surrogate fuel model usually contains one or more representative elements from important classes of compounds (alkane, alkene, aromatic, etc.) to represent the physical and chemical properties of real fuel that are of interest in engines. A reliable surrogate model used in CFD simulations can lead to a better understanding of the highly complex combustion processes involved in practical combustors, ultimately leading to combustor performance optimization [2]. 2,4,4-trimethyl-1-pentene (DIB-1), a C_8 iso-alkene, is one of the isomers of DIB that has gained significant attention as a representative of the alkene class of compounds in multi-component surrogate mechanisms [3-8]. A high-temperature chemical kinetic model describing DIB oxidation was published by Metcalfe et al. [3]. In the past decade, most surrogate models which include DIB have used the sub-mechanism proposed by Metcalfe et al. to simulate conditions outside the range of validation of the original DIB model. Thus, there is a need to update it.

In developing a detailed kinetic mechanism to describe DIB oxidation, there is a significant hierarchical dependence on the underlying isobutene chemistry on simulating high temperature experimental ignition delay times (IDTs) and laminar burning velocities (LBVs). The present authors started with the iC_4H_8 mechanism from Zhou et al. [1] to assess and address any deficiencies in this mechanism. Motivation leading to further development in iC_4H_8 kinetics is evident from Fig. 1(a), which shows poor quantitative predictions using the iC_4H_8 sub-model from Zhou et al. [1] compared to experimental data for DIB-1 from Hu et al. [9] at p = 1 atm and

T = 373 K and iC_4H_8 from [1] at p = 1 atm and T = 358 K, the peak flame speeds are under-predicted by 12 and 6 cm s^{-1} respectively. A recent iso-octane model from the literature [10] containing the previous iC_4H_8 model [1] exhibits relatively better agreement compared to iC_4H_8 and DIB-1, however the peak flame speed data for iso-octane from Ji et al. [11] is slightly under-predicted by ~1.5 cm s^{-1}. Particularly interesting are the experimental similarities in LBVs exhibited by iC_4H_8 and DIB-1 at 1 atm from Zhou et al. [1] and Hu et al. [9] respectively, indicates the strong dependence of DIB-1 kinetics on the underlying iC_4H_8 chemistry at high temperatures. Moreover, the kinetic analyses on the preliminary DIB model, as shown in the Fig. 2, suggested that the important decomposition pathways of DIB-1 at relatively higher temperatures produce either iC_4H_8 or its related radicals.

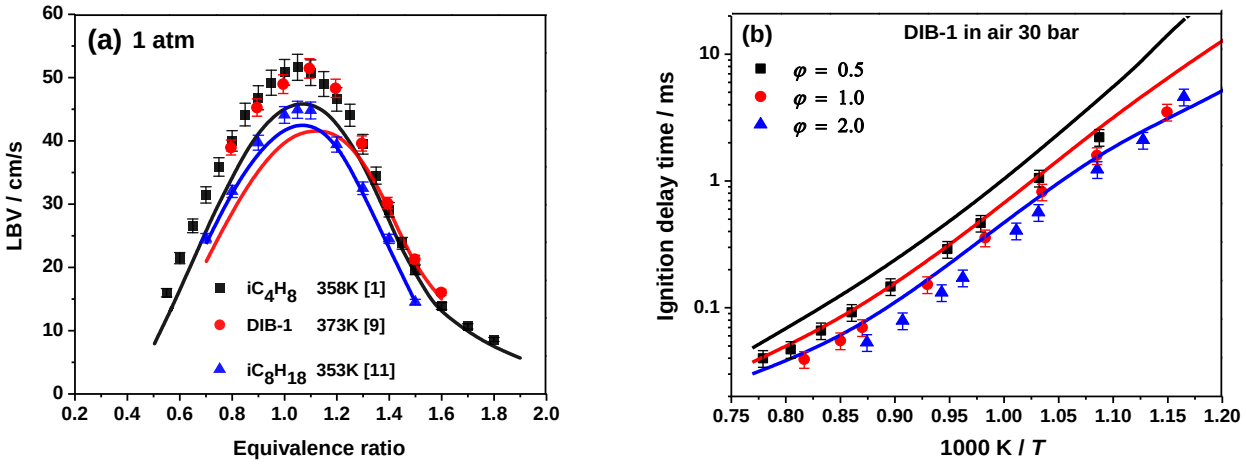

Figure 1: Performance of the kinetic models of iC_4H_8 [1], iso-octane [11] and DIB-1 (this study) using the iC_4H_8 kinetics from [1] for (a) LBV (b) DIB-1 IDT targets at various experimental conditions.

A similar under-prediction in the reactivity of DIB-1 is observed in Fig. 1(b) when validated against the IDTs at φ = 0.5, 1.0, 2.0 at p = 30 bar and at T = 900 – 1350 K. These new experiments were performed as part of a DIB-1 oxidation study in a high-pressure shock-tube (HPST) at NUIG and the data is attached as Supplementary material. This consistent under-prediction in the reactivity of the preliminary DIB model served as the prime motivation to revisit

iC_4H_8 kinetics. Moreover, we also aim to address several shortcomings in the previous iC_4H_8 model [1] to justify the completeness of the new detailed mechanism, since rate constants of several iC_4H_8 sensitive reactions, such as 2-methyl allyl ($i\dot{C}_4H_7$) radical recombination, are available in the literature [12]. The new iC_4H_8 model has been re-validated against the new LBV measurements taken at UCF at 1 atm and 428 K and against various other targets available in the literature. In addition, to determine the influence of the updated iC_4H_8 kinetics on the higher hydrocarbon model's performance, the high temperature targets of DIB-1 and iso-octane were also re-simulated.

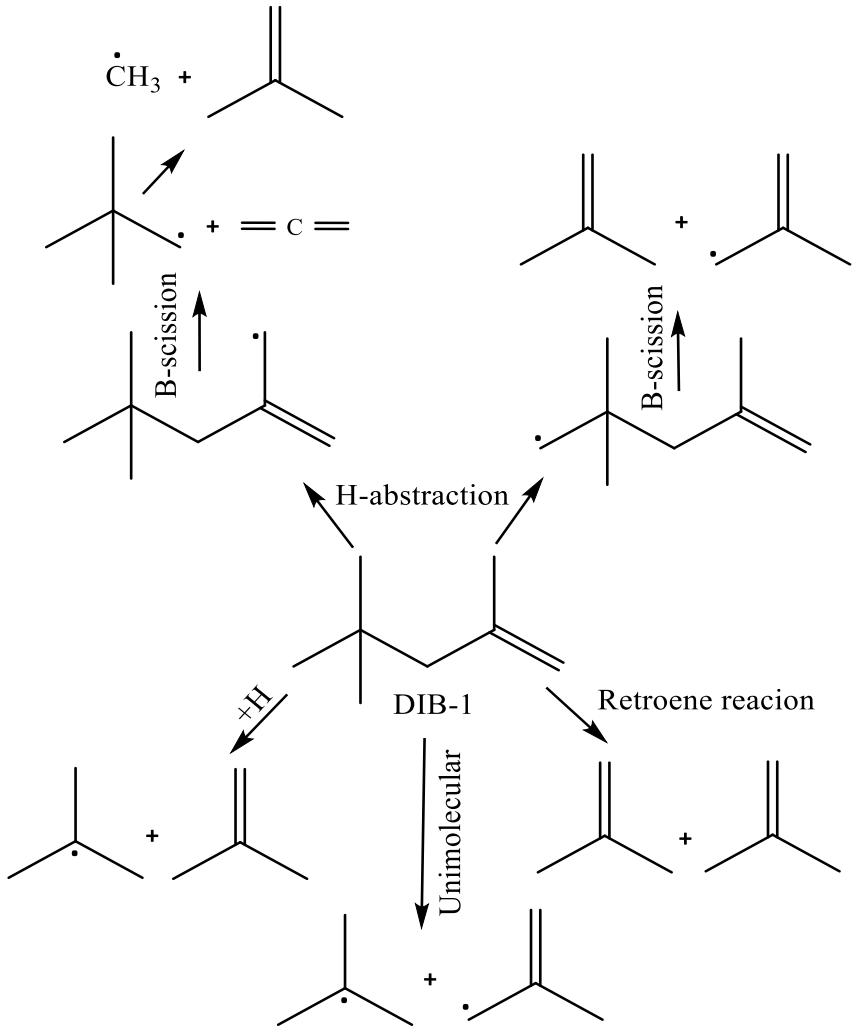

Figure 2: Various pathways in the current preliminary DIB-1 mechanism producing iC_4H_8 and/or its corresponding radicals.

2. Experimental

High pressure shock-tube (NUIG): The high pressure shock-tube facility at NUIG was discussed in detail by Nakamura et al. [13]. In the preparation of test mixtures, the fuel (DIB-1), O_2 and N_2, which were obtained from Sigma Aldrich and BOC Ireland, were added in the order of increasing partial pressure. The mixing tank and connecting manifold lines were maintained at 50 °C to prevent fuel condensation and the mixtures were allowed to mix diffusively for at least six hours to achieve homogeneity. The HPST facility at NUIG is a 9 m long steel tube with a uniform cross-section of 63.5 mm inner diameter. The test mixture is sent into the 'driven section' which is a 5.7 m long and a lighter non-reactive gas, helium is pressurized into a 3 m long 'driver section', which are separated by a 30 cm double-diaphragm section. A shock wave, formed by expansion of the driver gas due to the pressure difference created by the sudden evacuation of the He gas in the diaphragm section, propagates at supersonic speeds into the driven section, thereby heating and compressing the test mixture to the desired thermodynamic conditions before reaching the endwall. The arrival of the incident shock is monitored by six PCB pressure sensors mounted on the sidewall of the driven section to extrapolate the shock velocity to the endwall. The pressure history and the IDT of the test mixture are measured via a Kistler 603B pressure sensor mounted on the endwall. The compressed pressure and temperature conditions are calculated using the "reflected shock" routine in Gaseq [14] and the average uncertainties in T_C and in IDT measurements are 13 K and 25%, respectively [15].

Spherical bomb (UCF): The spherical experimental setup mainly consists of a combustion reaction environment, a mixture preparation system, optical instrumentation, data acquisition system, and ignition system, with details published elsewhere [16, 17]. The combustion reaction environment consists of a combustion chamber, a furnace, K-type thermocouples on the combustion chamber, and a dynamic pressure instrument. Briefly, the mixing tank was evacuated to less than 0.15 Torr before mixture preparation. Using the partial pressure method, isobutene (Sigma-Aldrich, 99%) and synthetic air (21% O_2 (Praxai, 99.999%) and 79% N_2 (Air Liquide,

99.999%)) mixture was prepared. The mixture was kept for five minutes to ensure stagnant status before the ignition. A minimum of three experiments were conducted for each equivalence ratio to verify repeatability. The constant volume method with a multi-zone thermodynamic model was used to calculate LBV. The detailed model was presented in [18, 19], with a brief explanation is provided here. Cantera [20] with AramcoMech3.0 [21] was used in equilibrium to calculate the thermodynamic properties of each burn zone during combustion. Following the solving properties of burned gases, LBV can be calculated from the measured pressure trace. Previous studies [22, 23] showed that the stretch effect is negligible in the constant volume method. Experimental data and flame propagation images are provided as Supplementary material. To calculate the LBV, linear extrapolation was used to get LBV at the initial temperature. To extrapolate, authors used two data in a stretch-free region before flame instability occurred. The average uncertainty in measured LBVs was found to be around 2.1%.

3. Kinetic Modeling

DIB model used in this study was developed in a collaborative effort between NUIG and LLNL and its kinetic description and analysis is beyond the scope of this paper, hence a paper focusing on detailed DIB kinetic model development and validation is currently under progress. In this section, we discuss the important updates done to the kinetics, thermodynamics and newly added pathways that were not present in the previous work of Zhou et al. for iC_4H_8 [1]. The foundation of the $C_0 - C_3$ base model used here is based on several prior mechanisms developed at NUI Galway. The kinetic parameters have been re-assessed by incorporating the rates and thermochemical properties from recent advances in the ab-initio studies and experimental diagnostics. The updated iC_4H_8 mechanism files, species dictionary and the high temperature version of the detailed $C_0 - C_4$ mechanism for LBV simulations are attached as Supplementary material.

3.1 Thermochemistry

Thermochemical data of the species in a mechanism are essential to estimate the reverse rate of the reactions and species properties such as enthalpy, entropy, heat capacity. In this study, the thermochemistry has been re-evaluated for all of the species that are of interest to iC_4H_8 combustion model using Benson's group additivity method in THERM software [24] based on the recent publication by Li and Curran [25] and Burke et al. [26]. Table 1 compares the thermodynamic properties of certain key species involved in the iC_4H_8 kinetic model and the updated THERM data for all species in this work are in good agreement compared to the literature data [27].

Table1. Comparison of thermodynamic properties of key iC_4H_8 species.

Species	Zhou et al. [1]			this work		
	H_f (kcal/mol)	S (cal/mol)	C_p/R	H_f (kcal/mol)	S (cal/mol)	C_p/R
$i\dot{C}_4H_7$	31.73	70.57	10.07	33.37	70.33	9.81
H15DE25DM	1.92	104.6	19.80	4.82	108.1	19.40
$tC_4H_9\dot{O}_2$	–23.56	86.96	15.90	–25.92	85.12	15.35
iC_4H_8O	–58.54	40.93	12.04	–30.20	71.35	12.69
cC_4H_8O	–52.07	42.07	11.24	–26.98	70.55	10.89
iC_4ketii	–70.71	99.15	15.79	–70.71	99.01	15.70
$i\dot{C}_4H_8O_2H$-t	–7.15	94.29	15.09	–6.31	96.91	14.59
$t\dot{C}_4H_8O_2H$-i	–9.24	88.92	15.38	–7.73	93.58	16.28
$ii\dot{C}_4H_7Q_2$-i	–25.88	115.3	19.61	–20.30	113.2	18.46

3.2 Newly updated reaction classes in the iC_4H_8 mechanism

Pyrolytic reactions: Unimolecular decomposition reactions involving C–C, C–H bond cleavage producing 1-methyl-vinyl ($\dot{C}_3H_5$-t), methyl ($\dot{C}H_3$) and methyl allyl ($i\dot{C}_4H_7$-i1) or 2-methyl allyl ($i\dot{C}_4H_7$) radicals and other bimolecular channels are included assuming analogous pressure dependent rates calculated at CCSD(T)/cc-pVTZ level of theory on propene potential energy surface by Ye et al. [28]. A comparison of rate constants for two key pyrolytic reactions between the two models is presented in Figs. 3(a) and 3(b). This class of reactions had a significant influence on the LBV predictions of iC_4H_8, which in turn influenced DIB-1 LBV predictions, will be discussed in detail in the following sections.

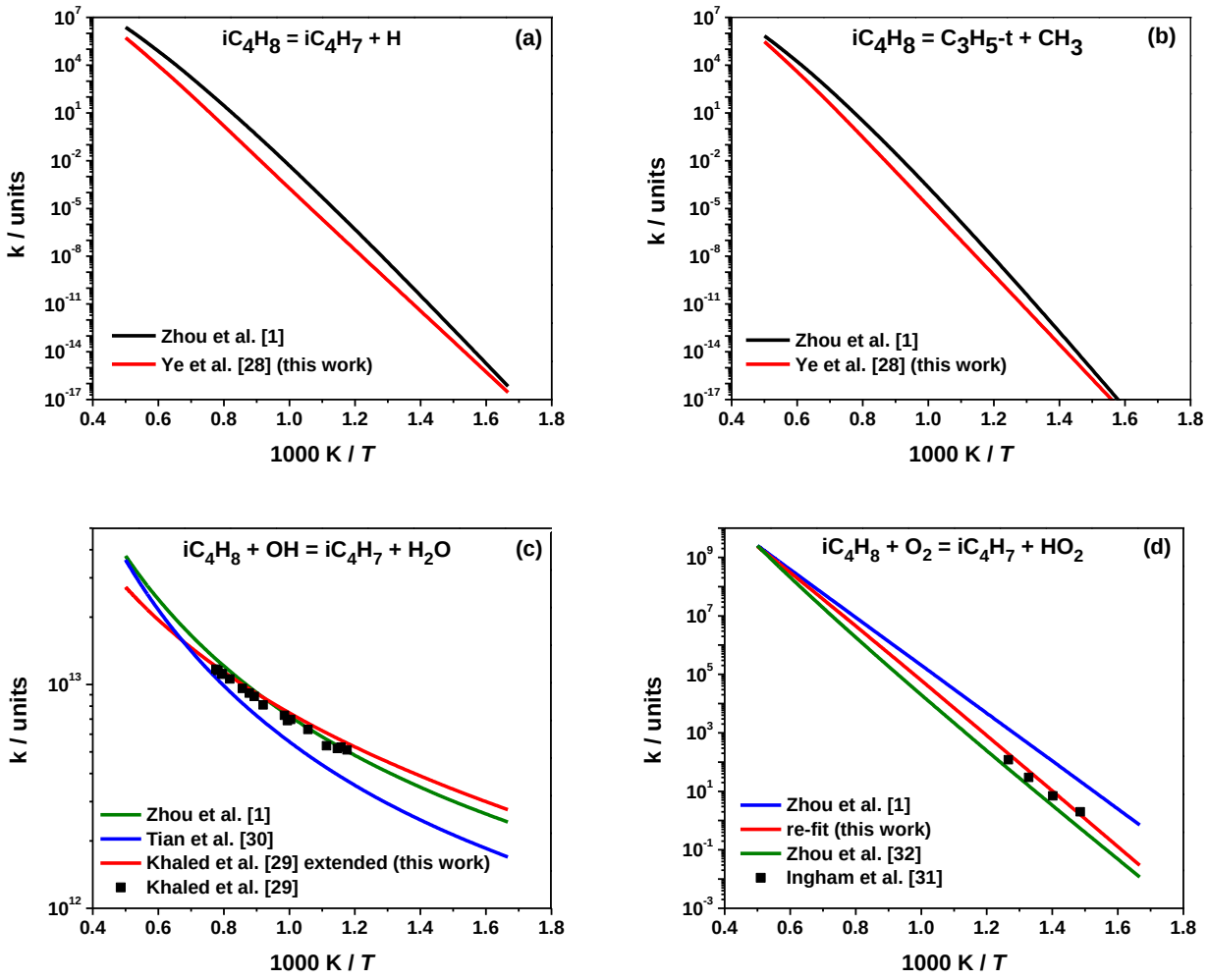

Figure 3: Rate constant comparison of pyrolytic and oxidation reactions for iC_4H_8 (a) iC_4H_8 = iC_4H_7 + H; (b) iC_4H_8 = C_3H_5-t + CH_3; (c) allylic H-atom abstraction $\dot{O}H$; (d) allylic H-atom abstraction O_2.

H-atom abstraction reactions*:* Rate constants for H-atom abstraction from primary allylic sites by ȮH, O_2 have been updated in this version. Figure 3(c) compares the rate constants for the H-atom abstraction by ȮH radicals which includes the direct measurements by Khaled et al. [29] and the theoretical calculations from Zhou et al. [1] and Tian et al. [30]. The H-atom abstraction rate constant by O_2 was re-fitted following the measurements by Ingham et al. [31] as shown in Fig. 3(d), which is approximately a factor of three higher in the temperature range 600 – 900 K compared to the theoretical calculations of Zhou et al. [32], whereas abstraction by hydroperoxyl ($H\dot{O}_2$) radicals remains unchanged and is taken from the calculations by Zádor et al. [33]. Rates for abstraction by Ḣ and Ö atoms and $\dot{C}H_3$ radicals are not available in the literature and hence analogies with propene [34-36] were taken and multiplied by two taking account of multiplicity.

$i\dot{C}_4H_7$ reactions: Pressure dependent rates for the recombination and dissociation reactions of resonantly stabilized $i\dot{C}_4H_7$ radicals were updated from the recent experimental study reported by Tranter et al. [12]. These reactions are significant inhibiting at low temperatures (650 – 950 K) and promoting at high temperatures (> 1200 K). A brief comparison of the allyl ($\dot{C}_3H_5$-a) and $i\dot{C}_4H_7$ recombination rates in the forward direction is depicted in Fig. 4(a). The $i\dot{C}_4H_7$ self-recombination rate in the previous model [1], is based on an analogy with allyl ($\dot{C}_3H_5$-a) radicals from Fridlyand et al. [37] with the A-factor is further reduced by a factor of 2.3 to accurately predict the IDT data at low temperatures (600 – 850 K). However, the direct measurements for the recombination of $i\dot{C}_4H_7$ [12] suggests that this rate is higher by at least a factor of 2 – 4 at low temperatures compared to $\dot{C}_3H_5$-a recombination rates [37-39].

The cycloaddition reactions of alkenyl-peroxy radicals are one of the important promoting channels in the LTC of olefins and the rate constants for cycloaddition of allylic iso-butenyl peroxy ($iC_4H_7\dot{O}_2$) radicals were updated from a recent high level calculation from Sun et al. [40] and the rate constant comparison plots are provided as Supplementary material.

Vinylic radical addition reactions: ȮH and HȮ$_2$ radical addition reactions were unchanged from the previous version [1]. However H-atom addition rates have been updated based on a recent ab-initio study (wB97XD/aug-cc-pVTZ) published by Power et al. [41], compared to the analogous propene rates from Miller et al. [35] in the previous model [1]. Figure 4(b) compares the rates for Ḣ atom addition.

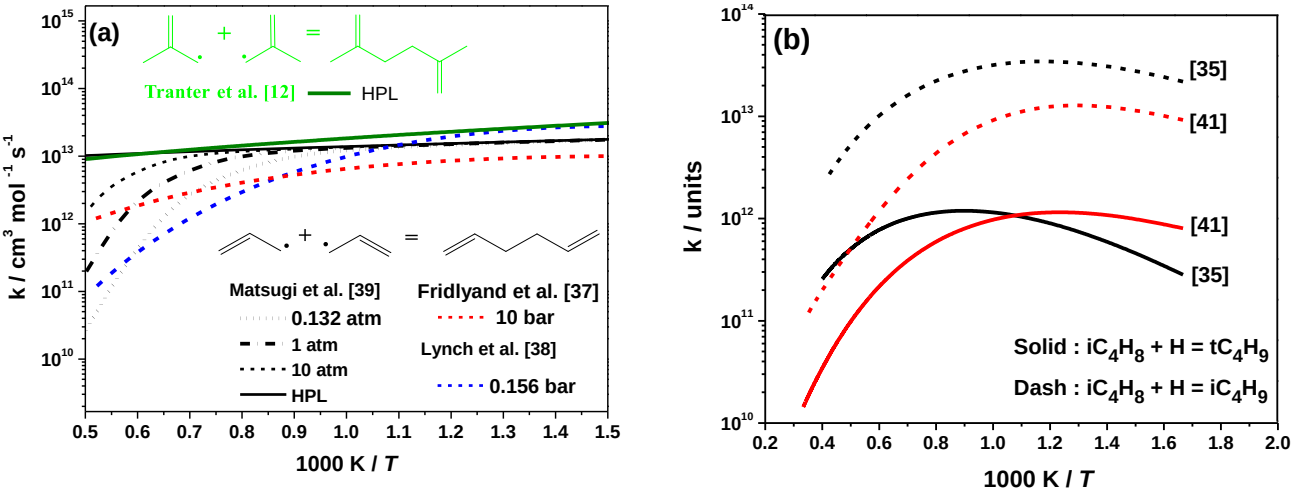

Figure 4: Rate constant comparison for (a) allylic radical recombination of iĊ$_4$H$_7$ and Ċ$_3$H$_5$-a (b) Ḣ-atom addition to iC$_4$H$_8$.

Waddington mechanism: The Waddington mechanism, proposed by Ray et al. [42], is a significant two-step alkene-specific rate promoting pathway at low to intermediate temperatures (600 – 950 K). In the previous iC$_4$H$_8$ model [1], the rates for the decomposition reactions involving the alkoxy radical (iQC$_4$H$_8$Ot) H$_2$OOHCȮC$_2$ producing CH$_3$COCH$_3$ + CH$_2$O + ȮH and CH$_3$COCH$_2$OOH + ĊH$_3$ were assumed by alkane analogy to Ċ$_3$CCOOH => iC$_4$H$_8$ + CH$_2$O + ȮH and Ċ$_2$CCOOH => H$_2$C=CHCH$_2$OOH + ĊH$_3$ from Villano et al. [43] respectively, to increase the reactivity to match IDT experiments at low temperatures. The previous iC$_4$H$_8$ model [1] estimates the allylic H-atom abstraction by O$_2$ rate to be a factor of 3 – 6 higher in the temperature range of 650 – 800 K, compared to the direct measurements of Ingham et al. [31]. This reaction inhibits reactivity in this temperature range and hence to counterbalance reactivity, the analogous alkane rates were employed for the alkoxy radical decomposition pathways. In this update, the alkane

analogy has been revoked and the specific Waddington-related rates from Sun et al. [44] were adopted to describe the Waddington mechanism. The rate constant comparison plots for the reactions discussed here are provided as Supplementary material.

<u>iĊ$_4$H$_7$-i1 reactions</u>: Pressure dependent rate constants for the methyl-allyl (iĊ$_4$H$_7$-i1) + O_2 reaction are adopted by analogy with a recent ab-initio study at the CCSD(T)-F12a/cc-pVTZ-F12//B2PLYPD3/cc-pVTZ level of theory for 2-methyl-vinyl (Ċ$_3$H$_5$-s) + O_2 by Chen et al. [45]. A sub-set of 11 elementary reactions were included in the current model compared to three pathways in the previous version [1] for which the rates were analogous to vinyl (Ċ$_2$H$_3$) + O_2 by Goldsmith et al [46]. This sub-set of reactions has very little influence on the iC$_4$H$_8$ model performance. However, it is important to note that proper kinetic treatment of these reactions is critical in simulating higher order alkenes.

At intermediate temperatures (750–1000 K), HȮ$_2$ radical concentrations are relatively high [33], and thus rates of recombination of HȮ$_2$ with allylic radicals are fast. Thus, we include the reactions of iso-butenyl hydroperoxyl (iĊ$_4$H$_6$OOH-i) and methyl-acrolein (iĊ$_3$H$_4$CHO-a) radicals with HȮ$_2$ in the mechanism with rate constants adopted by analogy with Ċ$_3$H$_5$-a + HȮ$_2$ as calculated by Goldsmith et al. [47].

3.3 iso-Butane sub-mechanism

The iso-butene kinetic mechanism is a subset of iso-butane chemistry, but the iso-butane model has not been validated in our previous iC$_4$H$_8$ model [1]. In this study, we updated all the kinetics and validated against IDT experiments in ST, RCM as shown in Fig 5.

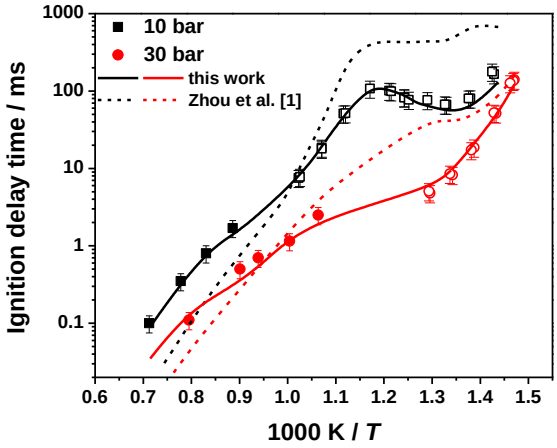

Figure 5: iso-Butane IDT experiments from [49] at 10 and 30 bar, compared against the current model as solid lines and that from [1] as dashed lines.

Additional validation plots of isobutane oxidation, such as LBVs and species profiles data from Baker et al. [48] using the current updated model are attached as Supplementary material. The agreement of the new model proposed in this study with the experimental results is excellent.

3.4 Simulation methods

The IDTs and species profiles were simulated using appropriate CHEMKIN PRO modules. LBVs were simulated maintaining the values of GRAD and CURV at 0.1 and using the mixture-averaged transport properties including the thermal diffusion (Soret effect) and all of the solutions were attained at a minimum of 400 grid points to confirm grid independence.

4. Results and discussion

4.1 Laminar burning velocities

Experimental and comparison of model performances for LBVs of iC_4H_8, iC_8H_{18} and DIB-1 are shown in Figs. 6(a) and 6(b). Of particular interest is the case of iC_4H_8, Fig. 6(a), the peak LBV predictions are improved by 1.5 – 3.5 cm s^{-1} at 1 atm and at unburned temperatures of 298 – 398 K compared to the previous model and experimental data [1]. In addition, the new iC_4H_8 model could well reproduce the new LBV experiments (presented as stars) performed for this study at 1 atm and an unburnt temperature of 428 K. However, experimental data on much of the

fuel-lean side is absent because it was difficult to ignite the iC_4H_8 mixture (without using other strategies for ignition). Notable in Fig. 6(b) are the improved DIB-1 LBV predictions with updated iC_4H_8 kinetics from this work, however iso-octane LBVs are over-predicted by ~1 cm s^{-1} at the peak. In addition, iC_4H_8 validation plots against the new LBV data from Movaghar et al. [50] at 8 – 30 atm and 400 – 520 K is provided as Supplementary material.

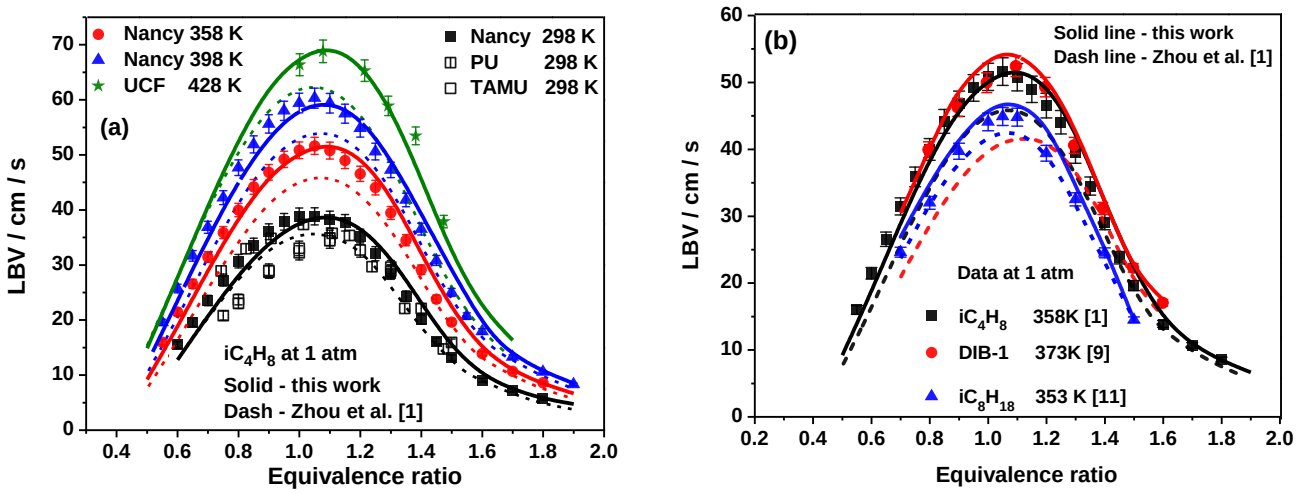

Figure 6: Improvement in LBV predictions using the updated iC_4H_8 kinetics (solid lines) and Zhou et al. [1] (dashed lines) for (a) iC_4H_8 (b) iC_8H_{18}, DIB-1 and iC_4H_8 at various conditions.

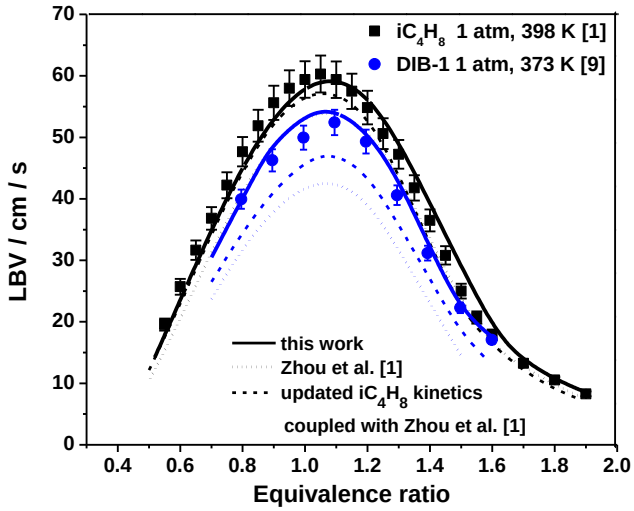

Figure 7: Comparison of the kinetics responsible for the improved LBV predictions of iC_4H_8 (black solids) and DIB-1 (blue circles). Dotted lines indicate iC_4H_8 model [1], Dashed lines are the updated iC_4H_8 kinetics from this work coupled with model from [1] and Solid lines are the updated C_0 – C_4 kinetics in this work.

The overall improvement of the LBV model predictions of iC_4H_8 which in turn influence the predictions of DIB-1 and iso-octane is due to the cumulative result of the updated C_0 – C_4 kinetics. To verify and highlight the sole effect of the iC_4H_8 specific kinetics on overall improvement of LBV predictions, a series of computational experiments were carried out. As represented in Fig. 7, Zhou et al. [1] (dotted line) severely under-predicts iC_4H_8 and DIB-1. By replacing only the iC_4H_8 kinetics developed here in the original isobutene mechanism [1], we observe a 3 and 6 cm s^{-1} increase in the peak flame speeds (dashed line) of iC_4H_8 and DIB-1 respectively. Interestingly in the case of DIB-1, C_0 – C_4 core mechanism is solely responsible for the overall improvement in the LBV predictions (dot to solid). The most sensitive iC_4H_8 reactions responsible for the improvement in LBV predictions are: $i\dot{C}_4H_7 + \dot{H} = \dot{C}_3H_5\text{-t} + \dot{C}H_3$ and $iC_4H_8 = i\dot{C}_4H_7 + \dot{H}$, whose rate constants are based on analogous propene reactions [28]. Considering the sensitivity of the two reactions at high temperatures for iC_4H_8 LBVs, these reactions could well be potential candidates for future work. The further improvement in the model performance (dash to solid) of iC_4H_8 and DIB-1 is attributed to accurate kinetic description of the underlying C_0 – C_3 chemistry in this study. Additional LBV validation plots for DIB-1 from Hu et al. [9] are provided as Supplementary material.

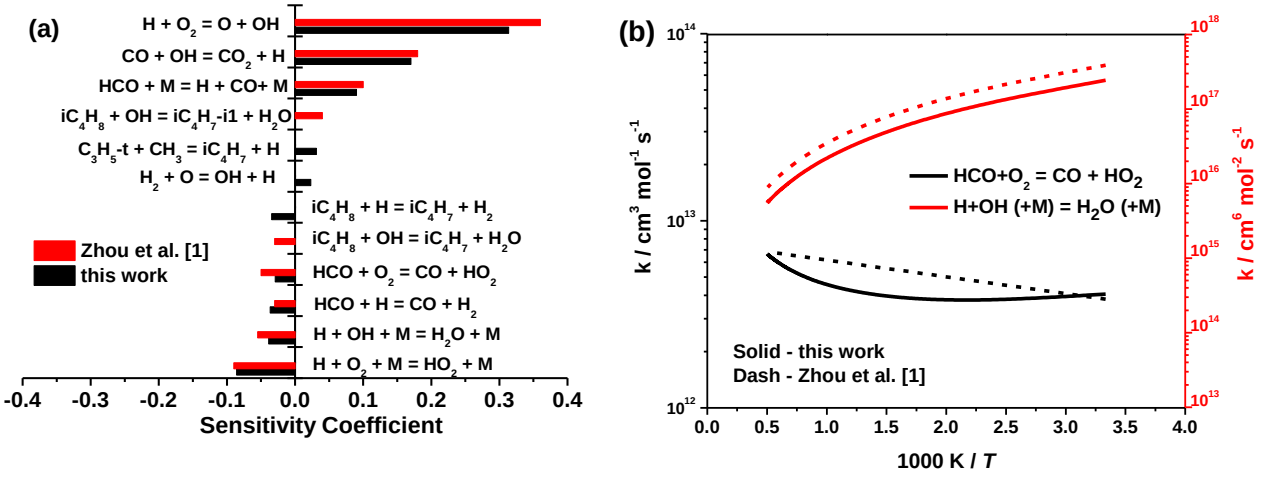

Figure 8: (a) Sensitive reactions in the previous [1] and current iC_4H_8 kinetics controlling LBVs at φ = 0.8 and 298 K (b) Rate constants comparison for the updated $H_2/H\dot{C}O$ kinetics.

Figure 8(a) compares the sensitive reactions using the latest and the previous iC_4H_8 model [1] that dictate flame speed reactivity and most of the reactions correspond to $C_0 – C_1$ chemistry. The updated iC_4H_8 kinetics highlighted in Fig. 8(a) are $i\dot{C}_4H_7 + \dot{H} = \dot{C}_3H_5\text{-t} + \dot{C}H_3$ and $iC_4H_8 + \dot{H} = i\dot{C}_4H_7 + H_2$. Few key H_2/CO reactions that were updated and highlighted in the sensitivity are $\dot{H} + \dot{O}H + M = H_2O + M$, $H\dot{C}O + O_2 = CO + H\dot{O}_2$ are represented in Fig. 8(b). Updating the H_2/CO kinetics is not only to improve iC_4H_8 flame speeds, but to attain consistency in the predictions of other key compounds in the base mechanism such as H_2, CH_4, C_2H_4, C_2H_6, C_3H_6, C_3H_8, etc. The rates of $H\dot{C}O + O_2 = CO + H\dot{O}_2$ and $\dot{H} + \dot{O}H + M = H_2O + M$ were updated to theoretical studies of Hsu et al. [51] and Sellevåg et al. [52], which are in good agreement with the experiments of Timonen et al. [53] and Srinivasan et al. [54] respectively.

4.2 Ignition delay times

The previous [1] and current iC_4H_8 models could well reproduce the iC_4H_8 IDT experiments, nonetheless, it is evident from Fig. 9(b) that improving the kinetic accuracy and consistency of iC_4H_8 kinetics had a positive effect on the IDT predictions of DIB-1, where iC_4H_8 is a critical intermediate. As shown in Fig. 9(a), the new model can well reproduce the experimental data [1] as well as the trend particularly in the low-temperature chemistry regime and the updated thermochemistry is responsible for between 5% and 10% of the total improvement in the model performance for specific IDT datasets. In the case of DIB-1 IDTs in the temperature range 900 – 1100 K, the new iC_4H_8 sub-model performs better than the previous model [1]. Additional iC_4H_8 [1] and DIB-1 [6] validation plots at several combustion relevant conditions are attached as Supplementary material.

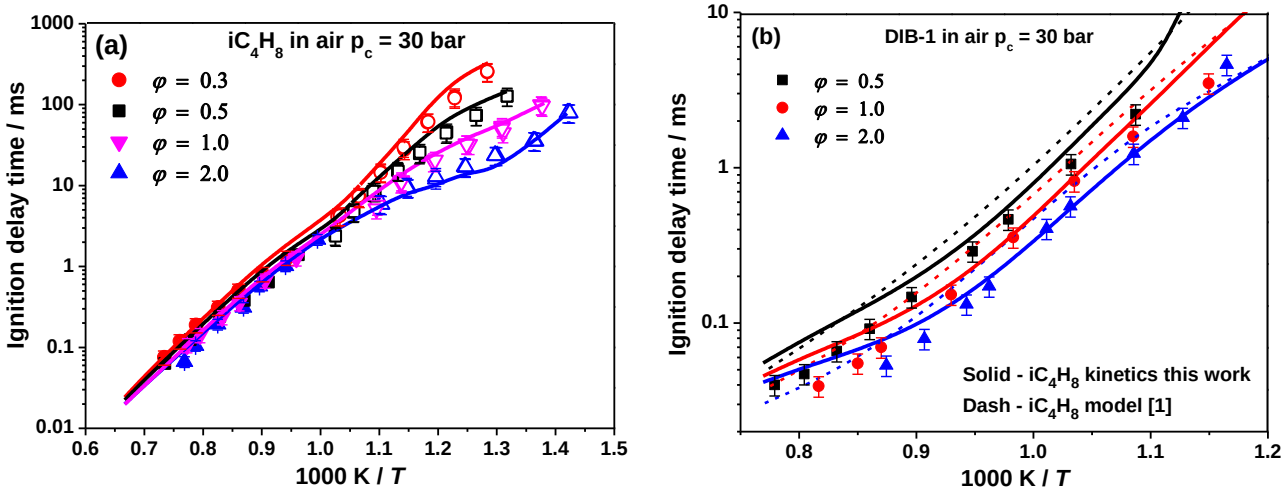

Figure 9: (a) Updated iC_4H_8 model validation for IDT targets (b) Influence of updated iC_4H_8 kinetics on DIB-1 IDT predictions.

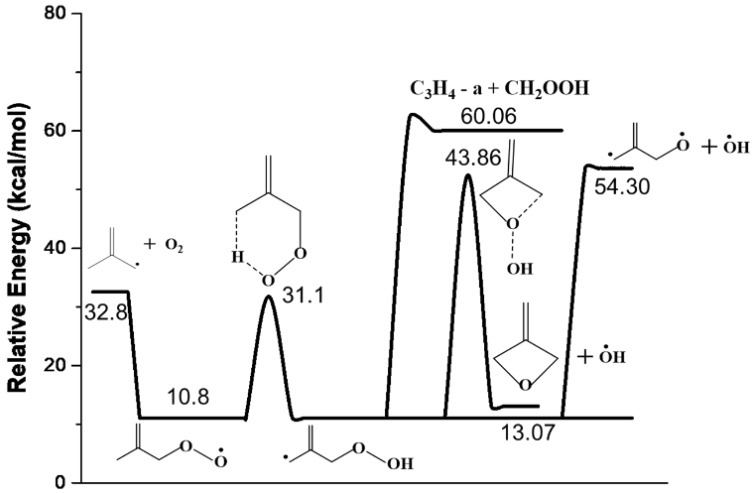

Figure 10: Potential energy diagram for 2-methyl allyl ($i\dot{C}_4H_7$) radical + O_2 reactions from Chen and Bozzelli [55].

The addition of methyl-allyl radical to O_2 is simulated according to the calculations of Chen and Bozzelli [55]. An abridged version of the $i\dot{C}_4H_7 + O_2$ potential energy surface (PES) investigated by Chen and Bozzelli [55] is shown in Fig. 10, and it can be seen that isomerization of $iC_4H_7\dot{O}_2$ to $i\dot{C}_4H_6OOH$-i proceeds through a barrier which is below the entrance channel, and the unimolecular decomposition channels of $i\dot{C}_4H_6OOH$-i exhibit very high activation energy barriers (~50 kcal mol^{-1}). Considering the similarities between the $i\dot{C}_4H_7$ and $i\dot{C}_4H_6OOH$-i

radicals, we have treated the kinetics of i$\dot{C}_4H_6$OOH-i radical consistent with those for 2-methyl allyl radical chemistry and include reactions of i$\dot{C}_4H_6$OOH-i with O_2 and $H\dot{O}_2$ radicals.

Figure 11 presents a comparison of the controlling chemistry for IDT predictions at φ = 1.0, p = 30 bar and T = 850 K for the previous [1] and the current iC_4H_8 models. Interestingly, the major promoting pathway in the new model is the updated cyclo-addition channel of methyl allyl peroxy radical (i$C_4H_7O_2$) producing CCYCCOOC-t1 from ref. [40], since its decomposition pathways produce CH_2O, CH_2CO, $H\dot{C}O$ and $\dot{C}H_3$ radicals that promote reactivity. According to the previous model [1], $\dot{C}_3H_5$-t oxidation reactions were very sensitive for iC_4H_8 IDT predictions in the temperature range 750 – 900 K, as the addition reactions of iC_4H_7 with $H\dot{O}_2$ proceeds via formation of $\dot{C}_3H_5$-t. The two C_3H_5-t reactions highlighted in the previous iC_4H_8 model, are $\dot{C}_3H_5$-t + O_2 producing CH_2O + $CH_3\dot{C}O$ and $CH_3CO\dot{C}H_2$ + Ö, are found to be insignificant according to the current iC_4H_8 model, as the current model adopts the rates calculated at a high-level theory for $\dot{C}_3H_5$-t oxidation by Chen et al. [45]. They noted that the major product channels of the reaction of $\dot{C}_3H_5$-t with O_2 are CH_2O + $CH_3\dot{C}O$, and the rates of formation of CH_2O + $CH_3\dot{C}O$ and $CH_3CO\dot{C}H_2$ + Ö are an order of magnitude lower than the estimated rates from Laskin et al. [56] assigned in the previous iC_4H_8 model [1]. Chen et al. verified the effect of these pathways on propene combustion using the mechanism published by Burke et al. [57] and found that implementing the calculated rates in the mechanism changes LBV predictions by approximately 10% at p = 1 and 50 atm in the temperature range of T_u = 300 – 900 K. These rates also alter IDT predictions by approximately 10 – 20% at p = 1 and 50 atm in the temperature range 700 – 1200 K at φ = 0.5 – 2.0 in air. The smaller effect of these reactions on propene combustion is due to the more favourable pathways at low temperatures, including H-atom abstraction from the allylic site producing methyl-allyl radicals and ȮH addition to the double bond and the subsequent reactions of the Waddington mechanism. However, in the case of C_4 iso-alkenes and larger ones, the dominant low temperature channels are the reactions of the daughter allylic radicals with $H\dot{O}_2$ which ultimately produce $\dot{C}_3H_5$-t radicals. Thus, an accurate kinetic description of $\dot{C}_3H_5$-t radical

is very important in predicting the high temperature kinetics of iso-olefins larger than C_3. It is interesting to note that $\dot{C}_3H_5$-t radical is not seen to be sensitive for propene kinetics [57]. Several other key reactions in the $C_0 – C_3$ model that employed estimates due to lack of availability of specific rates have been updated in the current version. A detailed flux analysis comparing the two models for iC_4H_8 oxidation is provided as Supplementary material at φ = 1.0, 850 K, 10 atm and 20% fuel consumption.

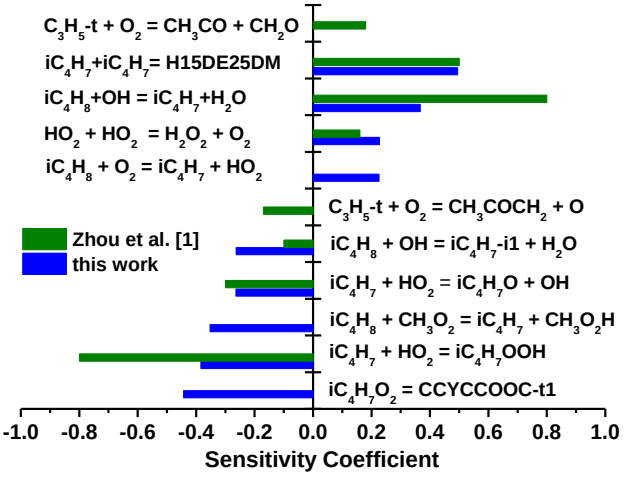

Figure 11: Sensitive iC_4H_8 reactions controlling IDTs for previous [1] and new iC_4H_8 models at φ = 1.0, p = 30 bar and T = 850 K.

4.3 Speciation data

The new model has been re-validated against the stable species profiles measured by Yasunaga et al. [58] for iC_4H_8 pyrolysis and Dagaut et al. [59] for iC_4H_8 oxidation, the model is in very good agreement with most of the species over wide range of experimental conditions provided in the respective papers as shown in Figs. 12 and 13, additional validation plots are attached as Supplementary material.

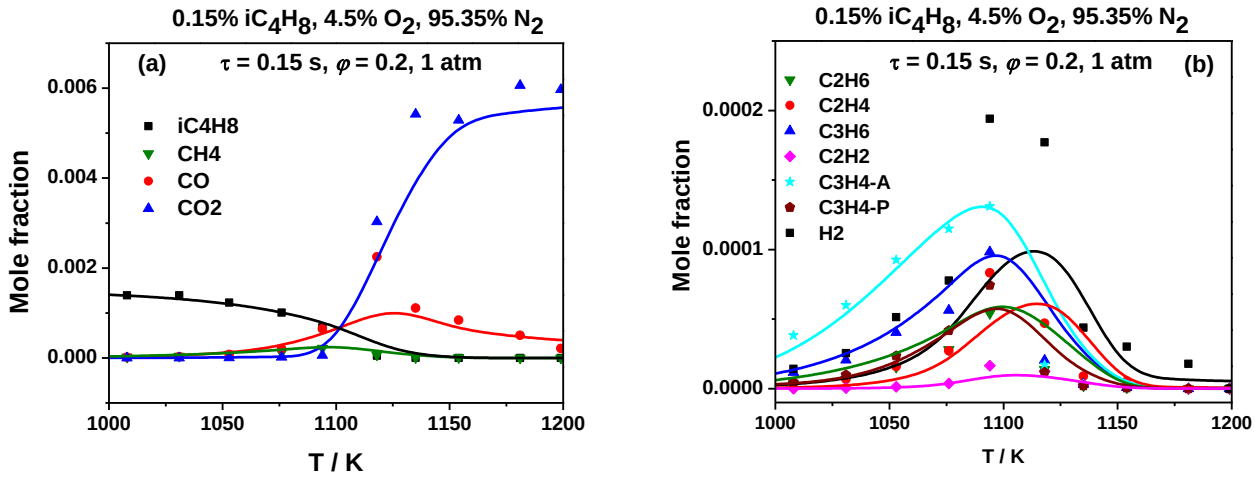

Figure 12: iC_4H_8 oxidation species profiles from Dagaut et al. [59] for 0.15% iC_4H_8, 4.5% O_2, 95.35% N_2 and φ = 0.2, at p = 1 atm and τ = 0.15 s. Points are experimental results, lines are current model predictions.

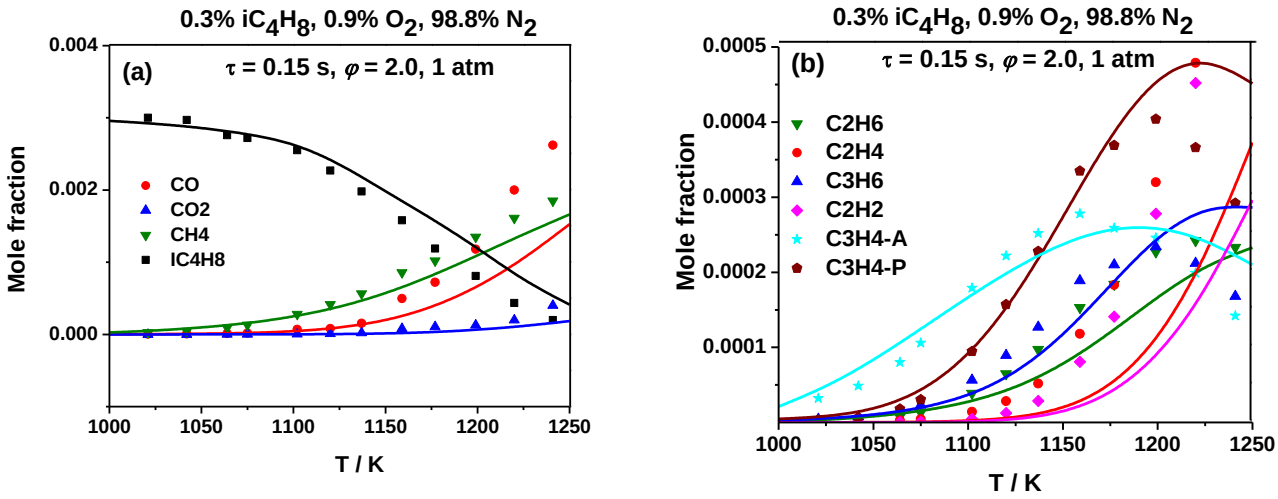

Figure 13: iC_4H_8 oxidation species profiles from Dagaut et al. [59] for 0.30% iC_4H_8, 0.9% O_2, 98.8% N_2 and φ = 2.0, at p = 1 atm and τ = 0.15 s. Points are experimental results, lines are current model predictions.

5. Conclusions

This paper emphasizes on the importance of accurate description of the C_0–C_4 kinetics to model higher hydrocarbons. Improving the kinetic accuracy of iC_4H_8 model improved not only iC_4H_8 predictions but also resulted in significant improvement in predictions of iso-octane and

DIB-1. The updated iC_4H_8 model no longer under-predicts the iC_4H_8 LBV experiments from ref. [1], furthermore, the new iC_4H_8 LBV experiments performed at UCF at 1 atm and 428 K are well reproduced by the current model. In addition, the current model is in very good agreement against variety of experimental targets over a wide range of conditions. The critical reactions responsible for majority of improvement of LBVs are $\dot{C}_3H_5$-t + $\dot{C}H_3$ = $i\dot{C}_4H_7$ + $\dot{H}$ and iC_4H_8 = $i\dot{C}_4H_7$ + $\dot{H}$. However, the rates were based on propene analogy and fundamental studies in their rates would be useful especially noticing its sensitivity on the LBVs.

A sensitivity analysis of IDT predictions highlighted the over-dependence of previous iC_4H_8 model [1] on the $\dot{C}_3H_5$-t oxidation, which has been rectified by adopting specific rates from Chen et al. [45]. In addition, the importance of cycloaddition pathways of alkenyl-peroxy radicals in the low temperature combustion of alkenes is highlighted. Several kinetic issues in the previous iC_4H_8 model [1] have been addressed in this article. Future work will be directed towards an updated and extensively validated kinetic mechanism for DIB isomers using the iC_4H_8 base chemistry developed in this work.

6. Acknowledgments

The authors at NUI Galway recognize funding support from Science Foundation Ireland (SFI) via their Principal Investigator Program through project number 15/IA/3177. UCF's effort is based upon work supported by the U.S. Department of Energy's Office of Energy Efficiency and Renewable Energy (EERE) under Award Number DE-EE0007984 (Co-Optima). This work at LLNL was performed under the auspices of the U.S. Department of Energy by Lawrence Livermore National Laboratory under Contract DE-AC52-07NA27344 as part of the Co-Optimization of Fuels & Engines (Co-Optima) project sponsored by the U.S. Department of Energy (DOE) Office of Energy Efficiency and Renewable Energy (EERE), Bioenergy Technologies and Vehicle Technologies Offices.

References

[1] C.-W. Zhou, Y. Li, E. O'Connor, K.P. Somers, S. Thion, C. Keesee, O. Mathieu, E.L. Petersen, T.A. DeVerter, M.A. Oehlschlaeger, G. Kukkadapu, C.-J. Sung, M. Alrefae, F. Khaled, A. Farooq, P. Dirrenberger, P.-A. Glaude, F. Battin-Leclerc, J. Santner, Y. Ju, T. Held, F.M. Haas, F.L. Dryer, H.J. Curran, A comprehensive experimental and modeling study of isobutene oxidation, Combust. Flame, 167 (2016), 353-379.
[2] W.J. Pitz, N.P. Cernansky, F.L. Dryer, F.N. Egolfopoulos, J.T. Farrell, D.G. Friend, H. Pitsch, Development of an Experimental Database and Chemical Kinetic Models for Surrogate Gasoline Fuels, SAE International, 2007.
[3] W.K. Metcalfe, W.J. Pitz, H.J. Curran, J.M. Simmie, C.K. Westbrook, The development of a detailed chemical kinetic mechanism for diisobutylene and comparison to shock tube ignition times, Proc. Combust. Inst., 31 (2007), 377-384.
[4] J.C.G. Andrae, Development of a detailed kinetic model for gasoline surrogate fuels, Fuel, 87 (2008), 2013-2022.
[5] L.R. Cancino, M. Fikri, A.A.M. Oliveira, C. Schulz, Ignition delay times of ethanol-containing multi-component gasoline surrogates: Shock-tube experiments and detailed modeling, Fuel, 90 (2011), 1238-1244.
[6] E. Hu, G. Yin, Z. Gao, Y. Liu, J. Ku, Z. Huang, Experimental and kinetic modeling study on 2,4,4-trimethyl-1-pentene ignition behind reflected shock waves, Fuel, 195 (2017), 97-104.
[7] H. Li, Y. Qiu, Z. Wu, S. Wang, X. Lu, Z. Huang, Ignition delay of diisobutylene-containing multicomponent gasoline surrogates: Shock tube measurements and modeling study, Fuel, 235 (2019), 1387-1399.
[8] S. Ren, S.L. Kokjohn, Z. Wang, H. Liu, B. Wang, J. Wang, A multi-component wide distillation fuel (covering gasoline, jet fuel and diesel fuel) mechanism for combustion and PAH prediction, Fuel, 208 (2017), 447-468.
[9] E. Hu, G. Yin, J. Ku, Z. Gao, Z. Huang, Experimental and kinetic study of 2,4,4-trimethyl-1-pentene and iso-octane in laminar flames, Proc. Combust. Inst., 37 (2019), 1709-1716.
[10] R. Fang, G. Kukkadapu, M. Wang, S.W. Wagnon, K. Zhang, M. Mehl, C.K. Westbrook, W.J. Pitz, C.-J. Sung, Fuel molecular structure effect on autoignition of highly branched iso-

alkanes at low-to-intermediate temperatures: Iso-octane versus iso-dodecane, Combust. Flame, 214 (2020), 152-166.
[11] C. Ji, S.M. Sarathy, P.S. Veloo, C.K. Westbrook, F.N. Egolfopoulos, Effects of fuel branching on the propagation of octane isomers flames, Combust. Flame, 159 (2012), 1426-1436.
[12] R.S. Tranter, A.W. Jasper, J.B. Randazzo, J.P.A. Lockhart, J.P. Porterfield, Recombination and dissociation of 2-methyl allyl radicals: Experiment and theory, Proc. Combust. Inst., 36 (2017), 211-218.
[13] H. Nakamura, D. Darcy, M. Mehl, C.J. Tobin, W.K. Metcalfe, W.J. Pitz, C.K. Westbrook, H.J. Curran, An experimental and modeling study of shock tube and rapid compression machine ignition of n-butylbenzene/air mixtures, Combust. Flame, 161 (2014), 49-64.
[14] C. Morley, Gaseq http://www.gaseq.co.uk/, (2004).
[15] M. Baigmohammadi, V. Patel, S. Martinez, S. Panigrahy, A. Ramalingam, U. Burke, K.P. Somers, K.A. Heufer, A. Pekalski, H.J. Curran, A Comprehensive Experimental and Simulation Study of Ignition Delay Time Characteristics of Single Fuel C1–C2 Hydrocarbons over a Wide Range of Temperatures, Pressures, Equivalence Ratios, and Dilutions, Energy & Fuels, 34 (2020), 3755-3771.
[16] G. Kim, B. Almansour, S. Park, A.C. Terracciano, K. Zhang, S. Wagnon, W.J. Pitz, S.S. Vasu, Laminar burning velocities of high-performance fuels relevant to the Co-Optima initiative, Advances and Current Practices in Mobility: SAE International Conference Proceedings, in press (2019).
[17] E. Ninnemann, G. Kim, A. Laich, B. Almansour, A.C. Terracciano, S. Park, K. Thurmond, S. Neupane, S. Wagnon, W.J. Pitz, S.S. Vasu, Co-optima fuels combustion: A comprehensive experimental investigation of prenol isomers, Fuel, 254 (2019), 115630.
[18] B. Almansour, G. Kim, S. Vasu, The Effect of Diluent Gases on High-Pressure Laminar Burning Velocity Measurements of an Advanced Biofuel Ketone SAE Int. J. Fuels Lubr., SAE International, 2018.
[19] B. Almansour, L. Thompson, J. Lopez, G. Barari, S.S. Vasu, Laser Ignition and Flame Speed Measurements in Oxy-Methane Mixtures Diluted With CO2, J. Energ. Resour-ASME, 138 (2015).
[20] D.G. Goodwin, H.K. Moffat, R.L. Speth, Cantera: An object-oriented software toolkit for chemical kinetics, thermodynamics, and transport processes, Caltech, Pasadena, CA, (2009).
[21] C.-W. Zhou, Y. Li, U. Burke, C. Banyon, K.P. Somers, S. Ding, S. Khan, J.W. Hargis, T. Sikes, O. Mathieu, E.L. Petersen, M. AlAbbad, A. Farooq, Y. Pan, Y. Zhang, Z. Huang, J. Lopez, Z. Loparo, S.S. Vasu, H.J. Curran, An experimental and chemical kinetic modeling study of 1,3-butadiene combustion: Ignition delay time and laminar flame speed measurements, Combust. Flame, 197 (2018), 423-438.
[22] A. Moghaddas, K. Eisazadeh-Far, H. Metghalchi, Laminar burning speed measurement of premixed n-decane/air mixtures using spherically expanding flames at high temperatures and pressures, Combust. Flame, 159 (2012), 1437-1443.
[23] E. Rokni, A. Moghaddas, O. Askari, H. Metghalchi, Measurement of Laminar Burning Speeds and Investigation of Flame Stability of Acetylene (C2H2)/Air Mixtures, J. Energ. Resour-ASME, 137 (2014).
[24] E.R. Ritter, THERM: a computer code for estimating thermodynamic properties for species important to combustion and reaction modeling, Journal of Chemical Information and Computer Sciences, 31 (1991), 400-408.
[25] Y. Li, H.J. Curran, Extensive Theoretical Study of the Thermochemical Properties of Unsaturated Hydrocarbons and Allylic and Super-Allylic Radicals: The Development and Optimization of Group Additivity Values, J. Phys. Chem. A, 122 (2018), 4736-4749.

[26] S.M. Burke, J.M. Simmie, H.J. Curran, Critical Evaluation of Thermochemical Properties of C1–C4 Species: Updated Group-Contributions to Estimate Thermochemical Properties, J. Phys. Chem. Ref. Data, 44 (2015), 013101.
[27] C.W. Gao, J.W. Allen, W.H. Green, R.H. West, Reaction Mechanism Generator: Automatic construction of chemical kinetic mechanisms, Comput. Phys. Commun., 203 (2016), 212-225.
[28] L. Ye, Y. Georgievskii, S.J. Klippenstein, Pressure-dependent branching in the reaction of 1CH2 with C2H4 and other reactions on the C3H6 potential energy surface, Proc. Combust. Inst., 35 (2015), 223-230.
[29] F. Khaled, B.R. Giri, A. Farooq, A high-temperature shock tube kinetic study for the branching ratios of isobutene+OH reaction, Proc. Combust. Inst., 36 (2017), 265-272.
[30] Z. Tian, J. Li, Y. Yan, Theoretical ab-initio kinetics of the reactions between isobutene plus hydroxyl, Chem. Phys. Lett., 720 (2019), 83-92.
[31] T. Ingham, R.W. Walker, R.E. Woolford, Kinetic parameters for the initiation reaction RH+O2→R+HO2, Symp. Combust., 25 (1994), 767-774.
[32] C.-W. Zhou, J.M. Simmie, K.P. Somers, C.F. Goldsmith, H.J. Curran, Chemical Kinetics of Hydrogen Atom Abstraction from Allylic Sites by 3O2; Implications for Combustion Modeling and Simulation, J. Phys. Chem. A, 121 (2017), 1890-1899.
[33] J. Zádor, S.J. Klippenstein, J.A. Miller, Pressure-Dependent OH Yields in Alkene + HO2 Reactions: A Theoretical Study, J. Phys. Chem. A, 115 (2011), 10218-10225.
[34] Y. Bedjanian, J. Morin, Reaction of O(3P) with C3H6: Yield of the Reaction Products as a Function of Temperature, J. Phys. Chem. A, 121 (2017), 1553-1562.
[35] J.A. Miller, S.J. Klippenstein, Dissociation of Propyl Radicals and Other Reactions on a C3H7 Potential, J. Phys. Chem. A, 117 (2013), 2718-2727.
[36] K. Wang, A.M. Dean, Chapter 4 - Rate rules and reaction classes, in: T. Faravelli, F. Manenti, E. Ranzi (Eds.), Comput. Aided Chem. Eng., Elsevier2019, pp. 203-257.
[37] A. Fridlyand, P.T. Lynch, R.S. Tranter, K. Brezinsky, Single Pulse Shock Tube Study of Allyl Radical Recombination, J. Phys. Chem. A, 117 (2013), 4762-4776.
[38] P.T. Lynch, C.J. Annesley, C.J. Aul, X. Yang, R.S. Tranter, Recombination of Allyl Radicals in the High Temperature Fall-Off Regime, J. Phys. Chem. A, 117 (2013), 4750-4761.
[39] A. Matsugi, K. Suma, A. Miyoshi, Kinetics and Mechanisms of the Allyl + Allyl and Allyl + Propargyl Recombination Reactions, J. Phys. Chem. A, 115 (2011), 7610-7624.
[40] X. Sun, W. Zong, J. Wang, Z. Li, X. Li, Pressure-dependent rate rules for cycloaddition, intramolecular H-shift, and concerted elimination reactions of alkenyl peroxy radicals at low temperature, PCCP, 21 (2019), 10693-10705.
[41] J. Power, K.P. Somers, C.-W. Zhou, S. Peukert, H.J. Curran, Theoretical, Experimental, and Modeling Study of the Reaction of Hydrogen Atoms with 1- and 2-Pentene, J. Phys. Chem. A, 123 (2019), 8506-8526.
[42] D.J.M. Ray, R. Ruiz Diaz, D.J. Waddington, Gas-phase oxidation of butene-2: The role of acetaldehyde in the reaction, Symp. Combust., 14 (1973), 259-266.
[43] S.M. Villano, L.K. Huynh, H.-H. Carstensen, A.M. Dean, High-Pressure Rate Rules for Alkyl + O2 Reactions. 2. The Isomerization, Cyclic Ether Formation, and β-Scission Reactions of Hydroperoxy Alkyl Radicals, J. Phys. Chem. A, 116 (2012), 5068-5089.
[44] H. Sun, J.W. Bozzelli, C.K. Law, Thermochemical and Kinetic Analysis on the Reactions of O2 with Products from OH Addition to Isobutene, 2-Hydroxy-1,1-dimethylethyl, and 2-Hydroxy-2-methylpropyl Radicals: HO2 Formation from Oxidation of Neopentane, Part II, J. Phys. Chem. A, 111 (2007), 4974-4986.
[45] X. Chen, C.F. Goldsmith, A Theoretical and Computational Analysis of the Methyl-Vinyl + O2 Reaction and Its Effects on Propene Combustion, J. Phys. Chem. A, 121 (2017), 9173-9184.
[46] C.F. Goldsmith, L.B. Harding, Y. Georgievskii, J.A. Miller, S.J. Klippenstein, Temperature and Pressure-Dependent Rate Coefficients for the Reaction of Vinyl Radical with Molecular Oxygen, J. Phys. Chem. A, 119 (2015), 7766-7779.

[47] C.F. Goldsmith, W.H. Green, S.J. Klippenstein, Role of O2 + QOOH in Low-Temperature Ignition of Propane. 1. Temperature and Pressure Dependent Rate Coefficients, J. Phys. Chem. A, 116 (2012), 3325-3346.
[48] R.R. Baker, R.R. Baldwin, R.W. Walker, Addition of i-butane to slowly reacting mixtures of hydrogen and oxygen at 480°C, Journal of the Chemical Society, Faraday Transactions 1: Physical Chemistry in Condensed Phases, 74 (1978), 2229-2251.
[49] D. Healy, N.S. Donato, C.J. Aul, E.L. Petersen, C.M. Zinner, G. Bourque, H.J. Curran, Isobutane ignition delay time measurements at high pressure and detailed chemical kinetic simulations, Combust. Flame, 157 (2010), 1540-1551.
[50] A. Movaghar, R. Lawson, F.N. Egolfopoulos, Confined spherically expanding flame method for measuring laminar flame speeds: Revisiting the assumptions and application to C1 - C4 hydrocarbon flames, Combust. Flame, 212 (2020), 79-92.
[51] C.C. Hsu, A.M. Mebel, M.C. Lin, Ab initio molecular orbital study of the HCO+O2 reaction: Direct versus indirect abstraction channels, J. Chem. Phys., 105 (1996), 2346-2352.
[52] S.R. Sellevåg, Y. Georgievskii, J.A. Miller, The Temperature and Pressure Dependence of the Reactions H + O2 (+M) → HO2 (+M) and H + OH (+M) → H2O (+M), J. Phys. Chem. A, 112 (2008), 5085-5095.
[53] R.S. Timonen, E. Ratajczak, D. Gutman, Kinetics of the reactions of the formyl radical with oxygen, nitrogen dioxide, chlorine, and bromine, The Journal of Physical Chemistry, 92 (1988), 651-655.
[54] N.K. Srinivasan, J.V. Michael, The thermal decomposition of water, Int. J. Chem. Kinet., 38 (2006), 211-219.
[55] C.-J. Chen, J.W. Bozzelli, Thermochemical Property, Pathway and Kinetic Analysis on the Reactions of Allylic Isobutenyl Radical with O2: an Elementary Reaction Mechanism for Isobutene Oxidation, J. Phys. Chem. A, 104 (2000), 9715-9732.
[56] A. Laskin, H. Wang, C.K. Law, Detailed kinetic modeling of 1,3-butadiene oxidation at high temperatures, Int. J. Chem. Kinet., 32 (2000), 589-614.
[57] S.M. Burke, W. Metcalfe, O. Herbinet, F. Battin-Leclerc, F.M. Haas, J. Santner, F.L. Dryer, H.J. Curran, An experimental and modeling study of propene oxidation. Part 1: Speciation measurements in jet-stirred and flow reactors, Combust. Flame, 161 (2014), 2765-2784.
[58] K. Yasunaga, Y. Kuraguchi, R. Ikeuchi, H. Masaoka, O. Takahashi, T. Koike, Y. Hidaka, Shock tube and modeling study of isobutene pyrolysis and oxidation, Proc. Combust. Inst., 32 (2009), 453-460.
[59] P. Dagaut, M. Cathonnet, Isobutene Oxidation and Ignition: Experimental and Detailed Kinetic Modeling Study, Combust. Sci. Technol., 137 (1998), 237-275.

Supplementary material:

File name	Contents
Experimental data.xlsx	New LBV and IDT experimental data
Flame propagation.pptx	Flame propagation images
Species dictionary.xlsx	Species identifiers
SMM.docx	Wide variety of validation for iC4 targets
NUIG Mech folder	Mechanism, Thermo, Transport files